RESEARCH ARTICLE

Colloid particle size-dependent dispersivity

Constantinos V. Chrysikopoulos[1] and Vasileios E. Katzourakis[2]

[1]School of Environmental Engineering, Technical University of Crete, Chania, Greece, [2]Department of Civil Engineering, Environmental Engineering Laboratory, University of Patras, Patras, Greece

Abstract Laboratory and field studies have demonstrated that dispersion coefficients evaluated by fitting advection-dispersion transport models to nonreactive tracer breakthrough curves do not adequately describe colloid transport under the same flow field conditions. Here an extensive laboratory study was undertaken to assess whether the dispersivity, which traditionally has been considered to be a property of the porous medium, is dependent on colloid particle size and interstitial velocity. A total of 48 colloid transport experiments were performed in columns packed with glass beads under chemically unfavorable colloid attachment conditions. Nine different colloid diameters and various flow velocities were examined. The breakthrough curves were successfully simulated with a mathematical model describing colloid transport in homogeneous, water-saturated porous media. The experimental data set collected in this study demonstrated that the dispersivity is positively correlated with colloid particle size, and increases with increasing velocity. The dispersivity values determined in this laboratory study were compared with 380 dispersivity values from earlier laboratory and field-scale solute, colloid and biocolloid transport studies published in the literature.

1. Introduction

Accurate prediction of contaminant and colloid transport in porous media relies heavily on usage of suitable dispersion coefficients. The widespread procedure for dispersion coefficient determination consists of conducting tracer experiments and subsequently fitting the collected breakthrough data with an advection-dispersion transport model. The fitted dispersion coefficient is assumed to characterize the porous medium and is often used thereafter to analyze experimental results obtained from the same porous medium with other solutes and colloids. The above described procedure inherently assumes that the dispersive flux of all solutes and colloids under the same flow field conditions is exactly the same. Consequently, this procedure should be avoided.

Numerous laboratory and field-scale studies have focused on estimation of either the longitudinal dispersion coefficient [*Harleman and Rumer*, 1963; *Pickens and Grisak*, 1981; *Koch and Brady*, 1985; *Han et al.*, 1985; *Chrysikopoulos et al.*, 1990; *Delgado*, 2006] or the transverse dispersion coefficient [*Delgado and Guedes de Carvalho*, 2000; *Cirpka et al.*, 2006; *Acharya et al.*, 2007; *Olsson and Grathwohl*, 2007]. Transverse dispersion is increasingly recognized as a controlling mass transfer mechanism for contaminant plume migration and NAPL dissolution in aquifers [*Chrysikopoulos et al.*, 1994; *Chrysikopoulos and Kim*, 2000; *Chrysikopoulos et al.*, 2003; *Rahman et al.*, 2005; *Cirpka et al.*, 2006; *Acharya et al.*, 2007; *Rolle et al.*, 2010]. Hydrodynamic dispersion coefficients are strongly dependent on interstitial fluid motion and molecular diffusion. Transverse dispersion coefficients are considerably smaller than longitudinal dispersion coefficients. Numerous correlations, which are typically derived from experimental observations, are available for the estimation of hydrodynamic dispersion coefficients for solute transport in porous media [*Delgado*, 2006, 2007; *Olsson and Grathwohl*, 2007]. Furthermore, theoretical and numerical procedures have been developed for the estimation of hydrodynamic dispersion coefficients for both periodic as well as heterogeneous porous media. Macroscopic dispersion is traditionally determined by averaging pore-scale simulations of dispersion, which are based on detailed descriptions of the pore structure [*van Milligen and Bons*, 2012; *Icardi et al.*, 2014]. For periodic porous media, dispersion coefficients may be determined with volume averaging and generalized Taylor-Aris-Brenner techniques, by defining a representative elementary volume (REV) [*Whitaker*, 1986; *Chrysikopoulos et al.*, 1992a, 1992b]. For nonperiodic or heterogeneous porous media, where REV selection

may not be a trivial task, random-walk particle tracking methods are often employed [*Salles et al.*, 1993; *Maier et al.*, 2000].

Considerable research efforts have focused on the influence of aquifer length scale on solute dispersivity. *Gelhar et al.* [1992] suggested that the longitudinal dispersivity increases linearly with scale and gradually approaches a constant asymptotic value. On the contrary, *Neuman* [1990, 1991] hypothesized that the longitudinal dispersivity continues to increase as long as the solute encounters heterogeneities of increasing length scales.

Solute molecular size can influence solute transport in porous media and can contribute to early breakthrough (breakthrough of larger solutes precedes that of smaller solutes), tailing (nonideal transport), and compound-dependent dispersion [*Brusseau*, 1993; *Hu and Brusseau*, 1994, 1995; *Chiogna et al.*, 2010]. Also, hydrodynamic dispersion coefficients must be used with caution because they can overestimate the amount of mixing (overlapping of initially adjacent but separated solute plumes) [*Semprini and McCarty*, 1991; *Acharya et al.*, 2007; *Olsson and Grathwohl*, 2007].

Previous studies have suggested that colloid transport in porous media is significantly affected by particle size [*Fontes et al.*, 1991, *Gannon et al.*, 1991]. Early breakthrough of colloids and biocolloids as compared to that of conservative tracers has been observed in several studies [*Bales et al.*, 1989; *Toran and Palumbo*, 1992; *Powelson et al.*, 1993; *Grindrod et al.*, 1996; *Dong et al.*, 2002; *Keller et al.*, 2004; *Vasiliadou and Chrysikopoulos*, 2011; *Sinton et al.*, 2012; *Syngouna and Chrysikopoulos*, 2013; *Chrysikopoulos and Syngouna*, 2014]. Colloid early breakthrough can be attributed to effective porosity reduction (colloids cannot penetrate smaller pores due to their inability to fit into them), preferential flow paths through high-conductivity regions, and exclusion from the lower-velocity regions [*Chrysikopoulos and Abdel-Salam*, 1997; *Dong et al.*, 2002; *Ginn*, 2002; *Ahfir et al.*, 2009], which can also be viewed as a reduction of the effective porosity of the porous medium [*Morley et al.*, 1998]. The finite size of a colloid particle excludes it from the slowest moving portion of the parabolic velocity profile within a fracture or a pore throat, thus the effective particle velocity is increased, while the overall particle dispersion is reduced compared to Taylor dispersion, but with a tendency to increase with increasing particle size over a certain range of particle diameters [*James and Chrysikopoulos*, 2000, 2003]. Exclusion of colloids from regions of lowest velocity can be modeled by particle tracking with truncated random distribution dispersive displacements [*Scheibe and Wood*, 2003]. Although the above mentioned studies have suggested that the transport of colloids and biocolloids is affected by particle size, the relationship between colloid particle size and dispersivity is not well understood.

The objective of this study was to evaluate the influence of colloid particle size and interstitial velocity on dispersivity. A large number of colloid transport experiments were performed in columns packed with glass beads. The experimental breakthrough data were fitted with an analytical colloid transport model. The estimated dispersivity values were compared to values published in the literature. Finally, arguments were made against generalization of results based on just a few experimental observations, which may lead to erroneous conclusions.

2. Background and Theoretical Considerations

2.1. Colloid Transport Model
The breakthrough data were fitted with the nonlinear least squares regression program ColloidFit, which employs the analytical colloid transport model derived by *Sim and Chrysikopoulos* [1995] and extended by *Thomas and Chrysikopoulos* [2007]. The model accounts for colloid transport in one-dimensional, homogeneous, water-saturated porous media with first-order attachment (or filtration) and inactivation. The objective of the nonlinear least squares method is to obtain estimates of the model parameters that minimize the residual sum of squares between simulated and observed data. In order for the effect of colloid size to be more easily discerned, the experimental conditions were simplified.

2.2. Hydrodynamic Dispersion and Dispersivity
The advection-dispersion equation is the most widely accepted model for describing solute and colloid transport in porous media. For one-dimensional porous media, the longitudinal hydrodynamic dispersion coefficient, D_L [L^2/t], is the sum of mechanical dispersion, D_m [L^2/t], and effective molecular diffusion, $\mathcal{D}_e$ [L^2/t]. The mechanical dispersion is the product of the interstitial velocity, U [L/t], raised to an empirical

constant n and the longitudinal dispersivity, α_L [L], whereas the effective molecular diffusion is the molecular diffusion coefficient, $\mathcal{D}_{AB}$ [L^2/t], divided by the tortuosity coefficient, $\tau \geq 1$. Therefore, the longitudinal hydrodynamic dispersion coefficient is generally expressed as [*Bear*, 1979]:

$$D_L = D_m + \mathcal{D}_e = \alpha_L U^n + \frac{\mathcal{D}_{AB}}{\tau} \tag{1}$$

Note that D_L frequently exhibits an almost linear dependence with interstitial velocity (i.e., $n \approx 1$). For a solute tracer, $\mathcal{D}_{AB}$ is determined using the Wilke-Chang relationship [*Wilke and Chang*, 1955]:

$$\mathcal{D}_{AB} = 7.4 \times 10^{-8} \frac{(\psi_B mw_B)^{1/2} T}{\mu_B V_A^{0.6}} \tag{2}$$

where A is the solute; B is the solvent (water); $\psi_B = \psi_{H2O} = 2.6$ is an association parameter for solvent B [*Bird et al.*, 2002]; $\mu_B = \mu_w = 0.890 \times 10^{-3}$ (N·s)/m^2 = 0.89 cp is the water dynamic viscosity at 25°C in units of centipoises (1 cp = 0.001 N·s/m^2), mw$_B$ = 18 g/mol is the molecular weight of water, T (K) is the absolute temperature, and $V_A = mw_A/\rho_A$ (cm^3/g mol) is the molar volume of solute A. For a spherical particle, $\mathcal{D}_{AB}$ is determined by the Stokes-Einstein diffusion equation [*Russel et al.*, 1989]:

$$\mathcal{D}_{AB} = \frac{k_B T}{3\pi\mu_B d_p} \tag{3}$$

where d_p [L] is the particle diameter, k_B [J/T] is Boltzmann's constant. The tortuosity is a fundamental property of a porous medium, which describes the interconnectedness of the pore space. Although several tortuosity models based on molecular diffusivity and electrical resistivity are available in the literature [*Garrouch et al.*, 2001], the model introduced by *Bruggeman* [1935] is frequently employed:

$$\tau = \theta^{1-\alpha} \approx \frac{1}{\sqrt{\theta}} \tag{4}$$

where $\alpha \approx 1.5$ is the Bruggeman exponent [*Pisani*, 2011], and θ is the porosity.

It has been clearly demonstrated in the literature, both experimentally and theoretically, that dispersivity is positively correlated with the scale of observation [*Pickens and Grisak*, 1981; *Gelhar and Axness*, 1983; *Neuman*, 1990]. One school of thought hypothesizes that α_L initially increases linearly with scale of observation and then gradually approaches a constant asymptotic value at an upper bound, which corresponds to the representative elementary volume (smallest volume of a porous medium over which measurements made are representative of the whole) [*Gelhar et al.*, 1992]. Another school of thought suggests that a single universal line can meaningfully describe the scaling relationship between α_L and displacement distance [*Neuman*, 1990]. The empirical power law that describes the α_L with scale of observation as a universal line or below the upper bound, is of the form:

$$\alpha_L = \xi(L)^\psi \tag{5}$$

where ξ [$L^{1-\psi}$] is a fitted parameter, and ψ is the scaling exponent or equivalently the slope of the fitted line on logarithmic paper (log-log plot).

3. Mathematical Development

3.1. Colloid Transport

There are several mathematical models available in the literature for colloid transport in porous media that rely on either continuum or statistical approaches. In this study, the frequently employed continuum approach was adopted [*Chrysikopoulos and Syngouna*, 2014]. The transport of colloids (including biocolloids) in one-dimensional, homogeneous, water-saturated porous media with first-order attachment (or filtration) and inactivation is governed by the following partial differential equation [*Sim and Chrysikopoulos*, 1995]:

$$\frac{\partial C(t,x)}{\partial t} + \frac{\rho_b}{\theta}\frac{\partial C^*(t,x)}{\partial t} = D_L\frac{\partial^2 C(t,x)}{\partial x^2} - U\frac{\partial C(t,x)}{\partial x} - \lambda C(t,x) - \lambda^*\frac{\rho_b}{\theta}C^*(t,x) \tag{6}$$

where C [M/L^3] is the concentration of colloids in suspension; C* [M/M] is the concentration of colloids attached on the solid matrix; t [t] is time; ρ_b [M/L^3] is the dry bulk density of the solid matrix; λ [$1/t$] is the transformation rate constant of colloids in solution (e.g., inactivation of suspended colloids); λ^* [$1/t$] is the transformation rate constant of attached colloids; and U [L/t] is the interstitial velocity, which may not be equal to the average colloid particle velocity.

The rate of colloid attachment onto the solid matrix is described by the following first-order equation [*Sim and Chrysikopoulos*, 1998, 1999]:

$$\frac{\rho_b}{\theta}\frac{\partial C^*(t,x)}{\partial t}=k_cC(t,x)-k_r\frac{\rho_b}{\theta}C^*(t,x)-\lambda^*\frac{\rho_b}{\theta}C^*(t,x) \tag{7}$$

where k_c [$1/t$] is the attachment rate constant, and k_r [$1/t$] is the detachment rate constant. The kinetic equation (7) is solved for C* subject to an initial condition of zero attached colloid concentration (C*(0,x) = 0) as follows:

$$C^*(t,x)=\frac{k_c\theta}{\rho_b}\int_0^t C(\tau,x)\exp\left[-\left(k_r\frac{\theta}{\rho_b}+\lambda^*\right)(t-\tau)\right]d\tau \tag{8}$$

For a semiinfinite one-dimensional porous medium in the presence of a colloid source in the form of an "instantaneous" pulse, the appropriate initial and boundary conditions are:

$$C(0,x)=0 \tag{9}$$

$$-D_L\frac{\partial C(t,0)}{\partial x}+UC(t,0)=M_\delta\delta(t) \tag{10}$$

$$\frac{\partial C(t,\infty)}{\partial x}=0 \tag{11}$$

where $M_\delta = M_{in}/A_c\theta$ [M/L^2] is the mass injected "instantaneously" over the cross-sectional area of the column (where M_{in} [M] is the injected mass, A_c [L^2] is the cross-sectional area of the porous medium), and $\delta(t)$ [$1/t$] is a modified Dirac delta function ($\delta(t = 0) = 1$, $\delta(t \neq 0) = 0$). Condition (9) establishes that there is no initial colloid concentration within the one-dimensional porous medium. The third or flux-type boundary condition (10) describes the influent flux, as an "instantaneous" pulse concentration [*Thomas and Chrysikopoulos*, 2007]. The downstream boundary condition (11) preserves concentration continuity for a semiinfinite system [*Chrysikopoulos et al.*, 1990].

The analytical solution to equations (6) and (8) subject to conditions (9)–(11) has been derived by *Thomas and Chrysikopoulos* [2007]:

$$
\begin{aligned}
C(t,x)=&\frac{M_\delta}{D_L^{1/2}}\exp\left[\frac{Ux}{2D_L}-Ht\right]\left\{\frac{1}{(\pi t)^{1/2}}\exp\left[\frac{-x^2}{4D_Lt}+\left(H-A-\frac{U^2}{4D_L}\right)t\right]\right.\\
&-\frac{U}{2D_L^{1/2}}\exp\left[\frac{Ux}{2D_L}+(H-A)t\right]\text{erfc}\left[\frac{x}{2(D_Lt)^{1/2}}+\frac{U}{2}\left(\frac{t}{D_L}\right)^{1/2}\right]\\
&+\int_0^t\frac{B\zeta}{\{B\zeta(t-\zeta)\}^{1/2}}I_1\left[2(B\zeta(t-\zeta))^{1/2}\right]\left\{\frac{1}{(\pi\zeta)^{1/2}}\exp\left[\frac{-x^2}{4D_L\zeta}+\left(H-A-\frac{U^2}{4D_L}\right)\zeta\right]\right.\\
&\left.\left.-\frac{U}{2D_L^{1/2}}\exp\left[\frac{Ux}{2D_L}+(H-A)\zeta\right]\text{erfc}\left[\frac{x}{2(D_L\zeta)^{1/2}}+\frac{U}{2}\left(\frac{\zeta}{D_L}\right)^{1/2}\right]\right\}d\zeta\right\}
\end{aligned}
\tag{12}
$$

where $A = k_c + \lambda$, $B = k_ck_r\theta/\rho_b$, $H = (k_c\theta/\rho_b) + \lambda^*$ [*Sim and Chrysikopoulos*, 1998], I_1 is the modified Bessel function of the first kind of order one, exp is the exponential function, erfc is the complementary error function, and ζ is a dummy integration variable. In this study, the experimental conditions were simplified as much as possible so that the effect of colloid size on the dispersivity is more easily discerned. Consequently, several parameters of the general colloid transport model can be fixed to zero

($k_c = k_r = \lambda = \lambda^* = 0$, and $A = B = H = 0$), and the mathematical model (6) reduces to the classical advection-dispersion equation.

3.2. Fitting Procedures

All fittings were conducted with the in-house developed nonlinear least squares regression software "ColloidFit," which incorporates the state of the art model-independent parameter estimation package "Pest" [*Doherty et al.*, 1994]. The software ColloidFit, among other statistics, is capable of calculating 95% confidence limits based on the variance-covariance matrix created during the fitting process, and uses a quadratic objective function:

$$S = \sum_{i=1}^{n} \left[w_i \left(C_i^{sim} - C_i^{exp} \right) \right]^2 \qquad (13)$$

where n (i = 1, ..., n) is the number of data, C_i^{exp} [M/L^3] is the ith measured concentration; C_i^{sim} [M/L^3] is the ith model simulated concentration; w_i is the ith weight (here $w_i = 1$). The criterion for convergence is that the weighted sum of squares does not change significantly from one iteration, p, to the next, p + 1. The convergence criterion employed here is: $\left| \left(S^p - S^{p+1} \right) / S^p \right| \le 0.01$

In all of the experiments conducted, only the two unknown model parameters U and D_L were estimated by fitting the analytical solution (12) with $k_c = k_r = \lambda = \lambda^* = 0$ to the experimental data. In general, fitting more than three unknown parameters is not recommended because for more than three unknown parameters, ColloidFit, as well as any other similar fitting code, may not provide unique estimates [*Katzourakis and Chrysikopoulos*, 2014], because the presence of many local minima may completely disorient the parameter upgrade vector from the global minimum. In this work, nonunique estimation problems are not expected because only two parameters were fitted at a time.

3.3. Moment Analysis

The tracer and colloid concentrations collected at the column exit were analyzed by the absolute temporal moments:

$$m_n(L) = \int_0^\infty t^n C(L, t) \, dt \qquad (14)$$

where the subscript n = 0, 1, 2, ... indicates the order of the moment, and L [*L*] is the porous medium (column) length. The zeroth absolute temporal moment, m_0 [tM/L^3], quantifies the total mass in the concentration distribution curve; the first absolute moment, m_1 [t^2M/L^3], describes the mean residence time; and the second absolute temporal moment, m_2 [t^3M/L^3], describes the degree of spreading of the concentration distribution curve. Also, the normalized temporal moments are defined as [*James and Chrysikopoulos*, 2011]:

$$M_n(L) = \frac{m_n(L)}{m_0(L)} = \frac{\int_0^\infty t^n C(L, t) dt}{\int_0^\infty C(L, t) dt} \qquad (15)$$

The first normalized temporal moment, M_1 [*t*], characterizes the center of mass of the concentration distribution curve and defines the average velocity. The second normalized temporal moment, M_2 [t^2], characterizes the spreading of the concentration distribution curve. Worthy of note is that the mass recovery, M_r, of the tracer or the suspended particles is quantified by the following expression:

$$M_r(L) = \frac{m_0(L)}{M_\delta / U} \qquad (16)$$

4. Materials and Methods

4.1. Packed Columns

Flowthrough experiments were conducted in glass columns with diameter 2.5 cm and length L = 15 or 30 cm, packed with spherical glass beads with diameter $d_c = 2$ mm. Each column was packed with glass beads under standing distilled deionized water (ddH$_2$O) to minimize air entrapment. Also, the glass beads

were poured into the column in small incremental volumes under gentle vibration to ensure that the columns were homogeneously packed. For each column, the dry bulk density (1.60–1.64 g/cm^3) and porosity (0.39–0.43) were determined. The columns were placed horizontally to minimize gravity effects [*Chrysikopoulos and Syngouna*, 2014]. A fresh column was packed for each experiment. Consequently, even for identical flow rates, small porosity variations will lead to slightly different interstitial velocities.

Following the procedure outlined by *Tong et al.* [2005], the glass beads were first rinsed sequentially with acetone and hexane and then soaked in concentrated HCl for about 12 h. Next, the beads were rinsed with ddH$_2$O until the water conductivity, as determined by a conductivity meter (Consort C931 electrochemical analyzer), was negligible. Subsequently, the glass beads were soaked in 0.1 *M* NaOH for 12 h, and rinsed repeatedly with ddH$_2$O until the ionic strength of water was negligible. Finally, the glass beads were dried in an oven at 105°C.

Sterile ddH$_2$O purified to a specific conductance of 0.05 μS/cm (ionic strength, I$_s$, of about 0.1 mM) with a Milli-Q UV plus water purification system containing a UV sterilization lamp (Millipore Corp., Massachusetts) was pumped from a flask into the column with a peristaltic pump. Several water flow rates, Q [L^3/t], ranging from 1 to 6 mL/min were employed in this study (see Table 1). The target pore water velocity or interstitial velocity was determined for each experiment (based on the flow rate set by the peristaltic pump, column porosity, and column cross-sectional area) and listed in Table 1. The tracer and colloid particle velocities were estimated by fitting procedures. Throughout the experiments, the temperature was maintained at 25 ± 1°C. All experiments were conducted under chemically unfavorable colloid attachment conditions (pH = 7, I$_s$ = 0.1 mM). Effluent samples were collected on preselected time intervals. Sample analysis was carried out immediately after the completion of each experiment. Finally, for each colloid breakthrough data set collected, the nonlinear least squares regression package ColloidFit was used to estimate the unknown model parameters.

4.2. Colloids and Tracer

Fluorescent polysterene microspheres (Duke Scientific Corp., Palo Alto, CA) with diameters d$_p$ = 28, 300, 600, 1000, 1750, 2100, 3000, 5000, and 5500 nm were used as model colloid particles. The concentration (number of particles/mL) of colloids injected into the column ranged from 10^7 to 10^{13} particles/mL, depending on the colloid size. Microsphere concentrations were measured by a fluorescence spectrophotometer (Cary Eclipse, Varian, Inc.). Each effluent colloid concentration was measured three times. Note that microspheres are sensitive to removal mechanisms such as straining (particle trapping in pore throats that are too small to allow particle passage) and wedging (particle attachment onto surfaces of two or more collector grains in contact). However, straining and wedging are not considered important mechanisms of mass loss in the packed columns examined in this study, because the colloid to collector diameter ratios (d$_p$/d$_c$) were well below the suggested threshold of 0.004 [*Johnson et al.*, 2010] or 0.003 [*Bradford and Bettahar*, 2006] for all cases examined (see Table 1). The colloids were inserted at the entrance of the column with a syringe (1–2 mL) in the form of an "instantaneous" pulse injection. The injected colloid mass for each experiment is listed in Table 1.

Bromide, in the form of NaBr, with density ρ_{NaBr} = 2.18 g/cm^3, was chosen as the nonreactive tracer for the transport column experiments. The nonreactive tracer experiments were conducted with 10^{-5} M NaBr. It should be noted that alkali halides are the most commonly used salts for subsurface fluid tracing [*Chrysikopoulos*, 1993]. Bromide concentrations were measured using ion chromatography (DX-500, Dionex Corp., Sunnyvale, CA).

5. Results and Discussion

For each colloid transport experiment conducted in this study, the fitted parameters U and D$_L$ were used for the determination of the corresponding longitudinal dispersivity. The values of the fitted model parameters U and D$_L$ as well as the value of the resulting α_L are listed in Table 1. A typical breakthrough curve obtained for colloids with d$_p$ = 1000 nm in a 30 cm column (experiment number 37) together with the corresponding tracer breakthrough curve (experiment number 3) are presented in Figure 1a. The experimental data are fitted with the analytical solution (curves) and the resulting dispersivities are: α_L = 0.10 cm for the tracer, and α_L = 0.36 cm for the colloids. Another set of breakthrough curves for colloids with d$_p$ = 5500 nm (experiment number 52) and corresponding tracer (experiment number 4) in a 30 cm column are also

Table 1. Experimental Conditions and Fitted Parameter Values

Experiment Number	L (cm)	d_p (nm)	ρ_b (g/mL)	M_{in} (μg)	Q (mL/min)	θ	$\mathcal{D}_e^a$ (cm²/min)	Fitted D_L^b (cm²/min)	Target U^c (cm/min)	Fitted U^d (cm/min)	α_L^e (cm)	Pe_m^f	M_r^g (%)
1	15	Tracer	1.69	1000	2	0.39	3.50×10^{-2}	0.16	1.04	0.99	0.12 ± 0.01	5.65×10^0	104.2
2	15	Tracer	1.69	1000	1	0.39	3.50×10^{-2}	0.07	0.52	0.50	0.06 ± 0.01	2.84×10^0	103.2
3	30	Tracer	1.59	400	4	0.39	3.50×10^{-2}	0.29	2.08	2.03	0.10 ± 0.01	1.16×10^1	95.0
4	30	Tracer	1.59	1000	4	0.41	3.50×10^{-2}	0.30	2.01	1.93	0.14 ± 0.01	1.10×10^1	97.5
5	15	28	1.69	20	1	0.41	4.09×10^{-4}	0.14	0.50	0.52	0.26 ± 0.02	2.53×10^2	110.0
6	15	28	1.69	20	2	0.42	4.09×10^{-4}	0.28	0.98	1.00	0.27 ± 0.02	4.89×10^2	99.9
7	15	28	1.69	20	2	0.41	4.09×10^{-4}	0.27	1.00	1.02	0.26 ± 0.01	5.00×10^2	99.5
8	15	28	1.69	20	4	0.41	4.09×10^{-4}	0.49	1.98	2.14	0.23 ± 0.01	1.05×10^3	101.2
9	15	28	1.69	20	6	0.40	4.09×10^{-4}	1.01	3.06	3.18	0.32 ± 0.01	1.55×10^3	99.4
10	15	28	1.69	20	6	0.41	4.09×10^{-4}	1.22	3.00	3.09	0.39 ± 0.05	1.51×10^3	97.4
11	15	600	1.69	10	1	0.43	1.91×10^{-5}	0.20	0.48	0.52	0.38 ± 0.03	5.41×10^3	101.4
12	15	600	1.69	10	4	0.41	1.91×10^{-5}	0.72	1.99	2.03	0.36 ± 0.03	$2.14 \times 10^{+4}$	89.1
13	15	600	1.69	10	2	0.41	1.91×10^{-5}	0.42	1.00	1.01	0.42 ± 0.03	$1.00 \times 10^{+4}$	83.1
14	15	600	1.69	10	6	0.41	1.91×10^{-5}	1.17	2.99	2.88	0.41 ± 0.02	$3.02 \times 10^{+4}$	99.4
15	15	1000	1.69	10	1	0.41	1.15×10^{-5}	0.14	0.50	0.51	0.29 ± 0.01	$8.68 \times 10^{+3}$	95.1
16	15	1000	1.69	10	2	0.40	1.15×10^{-5}	0.34	1.01	1.02	0.33 ± 0.01	$1.78 \times 10^{+4}$	98.1
17	15	1000	1.69	10	4	0.39	1.15×10^{-5}	0.65	2.08	2.09	0.31 ± 0.01	$3.63 \times 10^{+4}$	94.0
18	15	1000	1.69	10	6	0.41	1.15×10^{-5}	0.81	2.98	3.13	0.26 ± 0.01	$5.44 \times 10^{+4}$	99.5
19	30	28	1.59	20	1	0.40	3.96×10^{-4}	0.16	0.51	0.51	0.33 ± 0.02	$2.56 \times 10^{+2}$	107.0
20	30	28	1.59	20	4	0.41	3.96×10^{-4}	0.68	2.00	2.03	0.34 ± 0.03	$1.02 \times 10^{+3}$	105.0
21	30	28	1.59	20	4	0.41	3.96×10^{-4}	0.69	2.00	2.02	0.34 ± 0.03	$1.02 \times 10^{+3}$	103.1
22	30	28	1.59	20	6	0.41	3.96×10^{-4}	0.92	3.02	2.80	0.33 ± 0.02	$1.41 \times 10^{+3}$	99.9
23	30	28	1.59	20	2	0.41	3.96×10^{-4}	0.31	0.99	1.00	0.31 ± 0.03	$5.05 \times 10^{+2}$	104.0
24	30	28	1.59	20	6	0.39	3.96×10^{-4}	1.00	3.11	2.96	0.34 ± 0.03	$1.49 \times 10^{+3}$	107.0
25	30	28	1.59	20	1	0.42	3.96×10^{-4}	0.10	0.49	0.52	0.23 ± 0.01	$2.64 \times 10^{+2}$	93.3
26	30	28	1.59	40	4	0.41	3.96×10^{-4}	0.47	2.00	2.05	0.23 ± 0.01	$1.03 \times 10^{+3}$	101.6
27	30	28	1.59	20	4	0.40	3.96×10^{-4}	0.49	2.04	2.04	0.24 ± 0.01	$1.03 \times 10^{+3}$	101.2
28	30	300	1.59	20	2	0.41	3.70×10^{-5}	0.24	1.00	1.01	0.24 ± 0.01	$5.43 \times 10^{+3}$	98.7
29	30	300	1.59	20	4	0.41	3.70×10^{-5}	0.50	2.00	2.04	0.24 ± 0.02	$1.10 \times 10^{+4}$	102.6
30	30	300	1.59	20	4	0.40	3.70×10^{-5}	0.56	2.04	2.06	0.25 ± 0.03	$1.11 \times 10^{+4}$	98.4
31	30	300	1.59	20	2	0.40	3.70×10^{-5}	0.26	1.01	1.03	0.25 ± 0.03	$5.59 \times 10^{+3}$	97.6
32	30	600	1.59	20	2	0.41	1.85×10^{-5}	0.30	1.00	1.07	0.28 ± 0.03	$1.15 \times 10^{+4}$	92.6
33	30	600	1.59	20	4	0.41	1.85×10^{-5}	0.53	1.99	2.10	0.25 ± 0.02	$2.27 \times 10^{+4}$	96.7
34	30	600	1.59	20	4	0.40	1.85×10^{-5}	0.60	2.04	2.15	0.28 ± 0.03	$2.27 \times 10^{+4}$	95.9
35	30	1000	1.63	20	1	0.40	1.13×10^{-5}	0.19	0.51	0.50	0.38 ± 0.01	$8.81 \times 10^{+3}$	98.9
36	30	1000	1.63	20	2	0.40	1.13×10^{-5}	0.33	1.01	0.97	0.34 ± 0.01	$1.72 \times 10^{+4}$	101.0
37	30	1000	1.63	20	4	0.40	1.13×10^{-5}	0.71	2.03	2.03	0.36 ± 0.01	$3.58 \times 10^{+4}$	100.1
38	30	1000	1.63	20	2	0.40	1.13×10^{-5}	0.34	1.01	1.01	0.34 ± 0.02	$1.78 \times 10^{+4}$	106.0
39	30	1000	1.63	20	4	0.40	1.13×10^{-5}	0.79	2.04	2.01	0.39 ± 0.03	$3.55 \times 10^{+4}$	105.0
40	30	1000	1.63	20	4	0.40	1.13×10^{-5}	0.79	2.04	2.01	0.39 ± 0.03	$3.56 \times 10^{+4}$	105.0
41	30	1000	1.63	20	6	0.41	1.13×10^{-5}	1.04	3.01	3.03	0.34 ± 0.02	$5.36 \times 10^{+4}$	105.0
42	30	1750	1.63	20	3	0.42	6.46×10^{-6}	0.64	1.45	1.57	0.41 ± 0.02	$4.85 \times 10^{+4}$	97.8
43	30	1750	1.63	20	5	0.42	6.46×10^{-6}	1.11	2.41	2.60	0.43 ± 0.05	$8.05 \times 10^{+4}$	105.7
44	30	2100	1.63	20	5	0.40	5.39×10^{-6}	1.23	2.58	2.79	0.44 ± 0.03	$1.04 \times 10^{+5}$	99.5
45	30	2100	1.63	20	3	0.42	5.39×10^{-6}	0.69	1.46	1.58	0.43 ± 0.04	$5.84 \times 10^{+4}$	97.3
46	30	2100	1.63	20	5	0.40	5.39×10^{-6}	1.13	2.56	2.74	0.41 ± 0.02	$1.02 \times 10^{+5}$	102.0
47	30	3000	1.63	20	4	0.40	3.77×10^{-6}	0.79	2.06	1.94	0.41 ± 0.02	$1.03 \times 10^{+5}$	99.0
48	30	3000	1.63	20	4	0.40	3.77×10^{-6}	0.84	2.06	1.97	0.43 ± 0.03	$1.04 \times 10^{+5}$	98.0
49	30	3000	1.63	20	6	0.40	3.77×10^{-6}	1.18	3.09	2.90	0.41 ± 0.03	$1.56 \times 10^{+5}$	92.0
50	30	5000	1.63	20	4	0.41	2.26×10^{-6}	1.07	2.00	1.98	0.54 ± 0.02	$1.78 \times 10^{+5}$	85.6
51	30	5000	1.63	20	4	0.41	2.26×10^{-6}	1.14	1.97	2.03	0.56 ± 0.04	$1.79 \times 10^{+5}$	86.1
52	30	5500	1.63	20	4	0.41	2.03×10^{-6}	1.18	2.00	2.01	0.58 ± 0.02	$2.00 \times 10^{+5}$	92.5

[a]Effective molecular diffusion, $\mathcal{D}_e = \mathcal{D}_{AB}/\tau$: tracer evaluated with (2) and (4), and colloids with (3) and (4).
[b]Fitted hydrodynamic dispersion coefficient: fitted with ColloidFit.
[c]Target interstitial velocity, evaluated from the flow rate, Q: target U = Q/Aθ.
[d]Fitted tracer or colloid particle velocity: fitted with ColloidFit.
[e]Longitudinal dispersivity together with the associated 95% confidence intervals: evaluated with (1) by using fitted U, fitted D_L, and estimated $\mathcal{D}_e$, in conjunction with appropriate propagation of error estimation.
[f]Dimensionless Péclet number, $Pe_m = Ud_c/\mathcal{D}_e$.
[g]Mass recovery: evaluated with (16).

presented in Figure 1b, with resulting dispersivities: $\alpha_L = 0.14$ cm for the tracer, and $\alpha_L = 0.58$ cm for the colloids. Clearly, early breakthrough of colloids is observed in both cases presented in Figure 1. Also, the estimated tracer dispersivities are smaller than the corresponding colloid dispersivities. However, in Figure 1a,
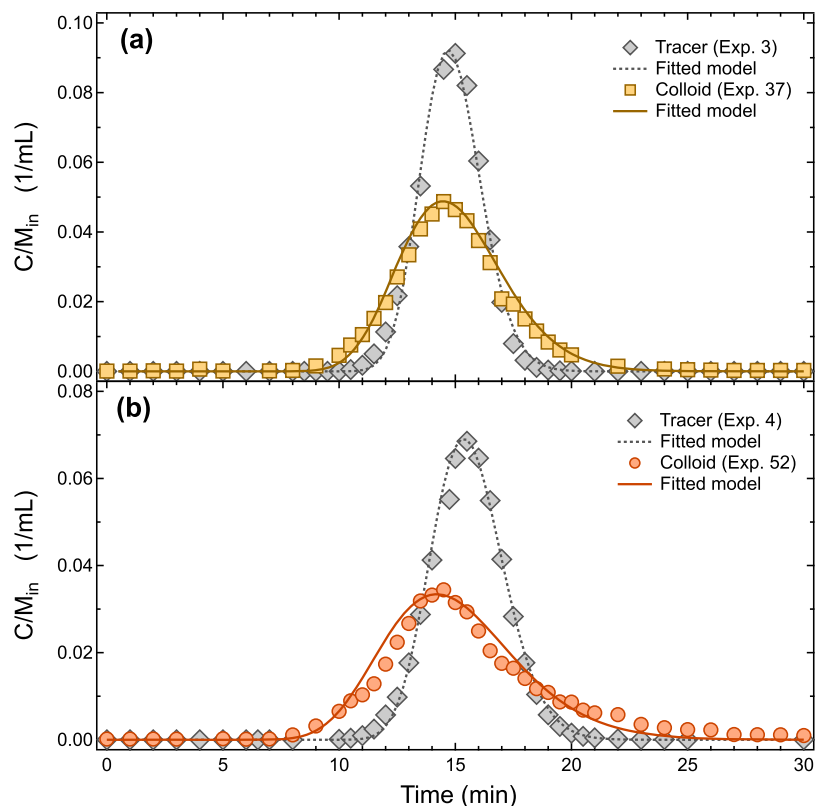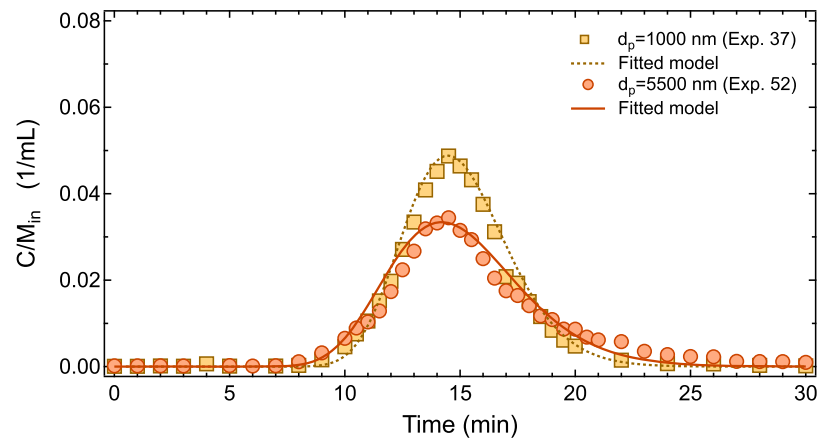
Figure 1. Breakthrough concentration data normalized with respect to M_{in}, for: (a) tracer (diamonds, $\alpha_L = 0.10$ cm) and colloids with $d_p = 1000$ nm (squares, $\alpha_L = 0.36$ cm) in a 30 cm column and (b) tracer (diamonds, $\alpha_L = 0.14$ cm) and colloids with $d_p = 5500$ nm (circles, $\alpha_L = 0.58$ cm) in a 30 cm column. The curves represent fitted model simulations for the tracer (dotted curves) and the colloids (solid curves).

both tracer and colloids flow with practically identical mean velocity, whereas in Figure 1b, the colloids travel a little faster than the tracer. This discrepancy can be attributed to variations in the combined effects of: (a) effective porosity reduction and (b) colloid exclusion from lower-velocity regions within the homogeneous porous media employed in this study, where the distribution of actual pore sizes is quite narrow. It should be noted that early breakthrough of the colloids is an expected result [e.g., *Grindrod et al.*, 1996; *Keller et al.*, 2004]. Furthermore, the breakthrough curves obtained for the transport experiments in a 30 cm column using colloids with $d_p = 1000$ nm (experiment number 37) and colloids with $d_p = 5500$ nm (experiment number 52) are presented in Figure 2. Note that the breakthrough of the larger colloids precedes that of the smaller colloids, and the corresponding dispersivities are: $\alpha_L = 0.36$ cm for the colloids with $d_p = 1000$ nm, and $\alpha_L = 0.58$ cm for the colloids with $d_p = 5500$ nm. Also, larger colloids spread more, and yield a smaller peak concentration compared to the smaller colloids. Certainly, the experimental data presented in Figures 1 and 2 suggest that colloid dispersivity is dependent on colloid particle size.

The relationship between dispersivity and colloid particle size is further explored by plotting in Figure 3 all of the longitudinal dispersivity values determined in this study against colloid diameter. For comparison, tracer dispersivities are also presented in Figure 3. Clearly, there is an obvious trend of dispersivity with increasing colloid particle diameter. Subsequently, the data presented in Figure 3 were statistically analyzed. The H_0 hypothesis that the population regression is linear was accepted, and the F test's hypothesis that the slope is zero was rejected. The F tests were conducted with the graphical statistical software "IGOR-Pro" (WaveMetrics Inc.). To quantify the relationship between the dispersivity and the size of colloid diameter, the average of the various longitudinal dispersivity values, for each colloid particle diameter available, were plotted against the colloid diameter in Figure 4, together with the standard regression line. Clearly, there is a positive correlation between α_L and d_p, which is of the form:

Figure 2. Breakthrough concentration data normalized with respect to M_{in}, for the colloids with $d_p = 1000$ nm (squares) and the colloids with $d_p = 5500$ nm (circles). The experiments were conducted in a 30 cm column. The curves represent fitted model simulations for the colloids with $d_p = 1000$ nm (dotted curve) and $d_p = 5500$ nm (solid curve). Here $\alpha_L = 0.36$ cm for the colloids with $d_p = 1000$ nm, and $\alpha_L = 0.58$ cm for the colloids with $d_p = 5500$ nm.

$$\alpha_L[cm] = 0.29 + 5.34 \times 10^{-5} \ d_p[nm] \tag{17}$$

Note that the preceding correlation predicts the longitudinal dispersivity in cm, and the colloid diameter should be in units on nm. This correlation is not recommended for the estimation of tracer dispersivity. However, at the limit of $d_p = 0$, the above correlation yields a dispersivity value within a factor of 2 to 3 from the experimentally determined tracer dispersivities (see Table 1).

The observed increase in α_L is attributed to the combined effects of reduction of the colloid effective porosity that leads to tortuosity changes, possible existence of preferential flow paths, and exclusion from the lower-velocity regions. Thus, some colloids are getting slowed down having to pass through small pore spaces, where other colloids are managing to stay in fast flow paths. This result is in agreement with the work published by *Jourak et al.* [2013] who studied theoretically the effects of particle-size distribution on the longitudinal dispersion coefficient in models of packed columns, and the work published by *Bennacer et al.* [2013] who investigated experimentally the transport and deposition of suspended particles with different size distributions in water-saturated porous media. However, *Keller et al.* [2004], *Vasiliadou and Chrysikopoulos* [2011], and *Syngouna and Chrysikopoulos* [2011] reported that α_L decreases with increasing d_p. These contradictory findings are probably due to the very limited number of experimental data used, and the experimental conditions that led to significant mass retention caused by straining and/or attachment.
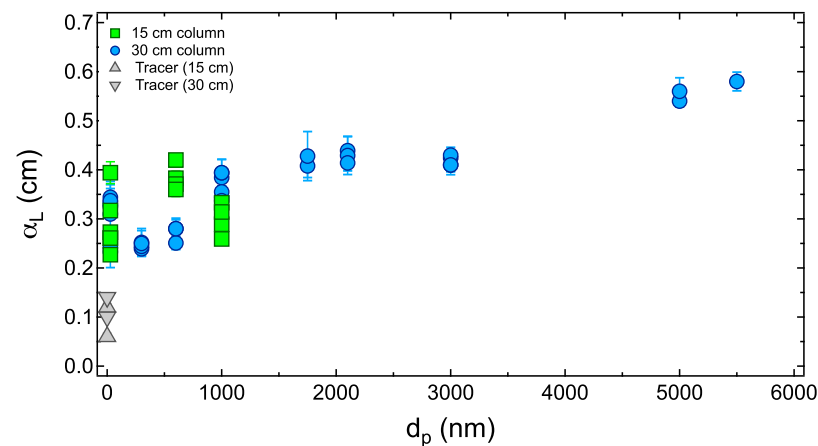

Figure 3. Longitudinal dispersivities from all 48 colloid transport experiments conducted in this study. The squares represent colloid transport experiments conducted in 15 cm columns, the circles represent colloid transport experiments conducted in 30 cm columns, and the triangles represent tracer transport resperiments. Error bars not shown are smaller than the size of the symbol.
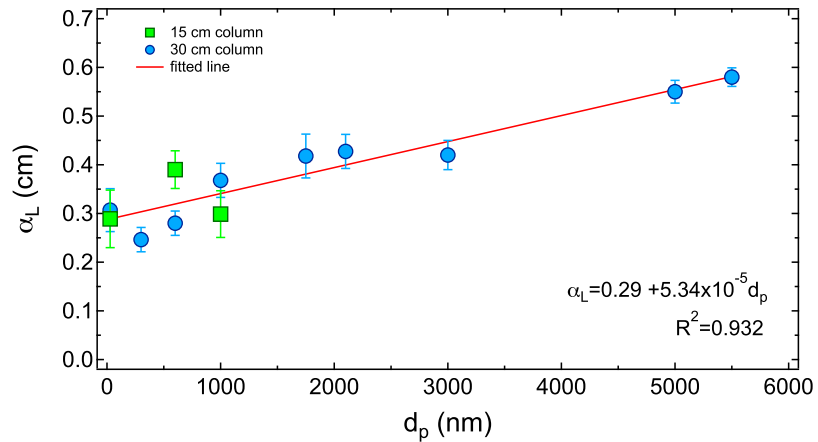
Figure 4. Averaged longitudinal dispersivity as a function of colloid particle diameter. The squares represent colloid transport experiments conducted in 15 cm columns, the circles colloid transport experiments conducted in 30 cm columns, and the solid line is a standard linear regression line.

The velocity enhancement of colloid particles, which is often observed in studies of colloid and biocolloid transport in fractures and micromodels, is commonly attributed to colloid exclusion from the lower-velocity regions [*James and Chrysikopoulos*, 2003; *Auset and Keller*, 2004]. However, in porous media, in addition to colloid exclusion from the lower-velocity regions [*Scheibe and Wood*, 2003], colloid particles experience a substantial reduction of the effective porosity [*Morley et al.*, 1998], as illustrated in Figure 5. Essentially, the volume of void-space accessible by colloids or colloid effective porosity decreases as the particle size of the colloids increases, because colloids do not enter pore spaces with opening smaller than d_p. However, under
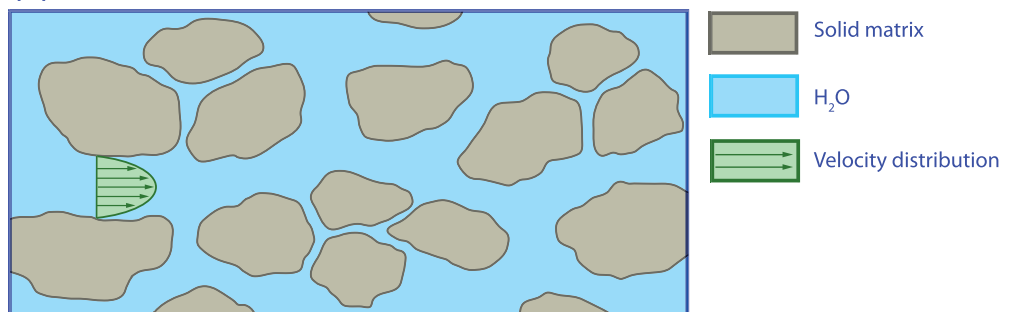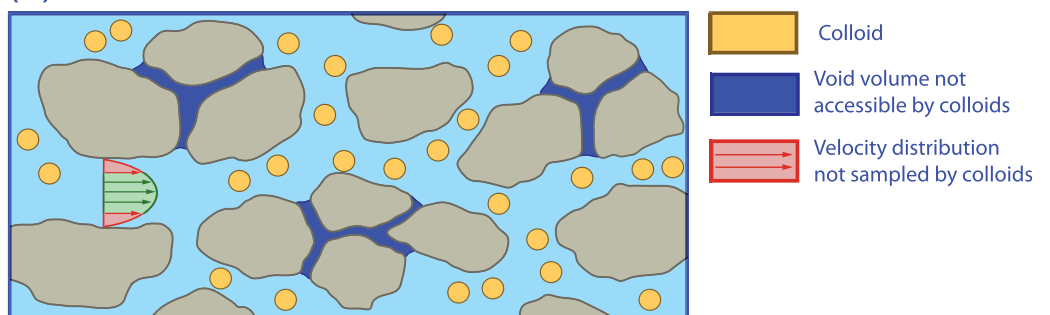

Figure 5. Schematic illustration of (a) tracer (conservative solute) and (b) colloid transport in water-saturated porous media. The tracer can sample the entire velocity spectrum within the parabolic profile (green region). Colloids do not sample the truncated portion of the parabolic velocity profile (red region). Also, colloids do not enter pore spaces with opening smaller than d_p, which essentially leads to reduction of the volume of void-space accessible by colloids (reduction of the colloid effective porosity). Under the experimental conditions of this study, the interstitial fluid has continuous access to the entire volume of void-space.
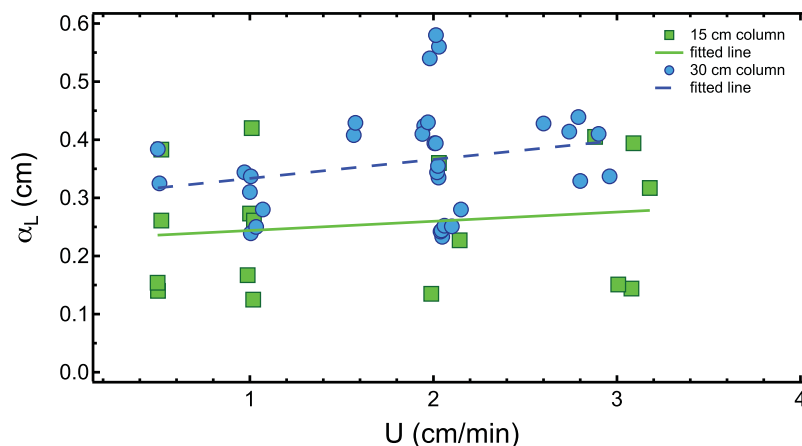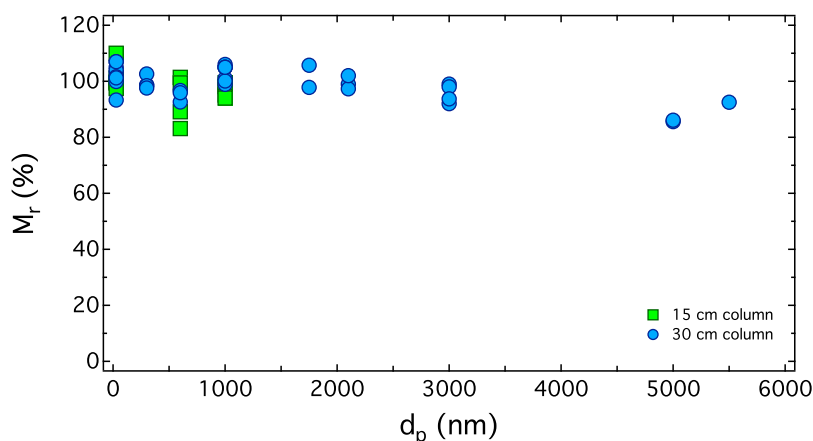
Figure 6. Longitudinal dispersivity as a function of interstitial velocity. The squares represent colloid transport experiments conducted in 15 cm columns, the circles colloid transport experiments conducted in 30 cm columns, the solid line is a standard linear regression line for the experiments conducted in the 15 cm column, and the dashed line for the experiments conducted in the 30 cm column.

the experimental conditions of this study (chemically unfavorable colloid attachment conditions, absence of straining and wedging), the interstitial fluid has continuous access to the entire volume of void-space. Note that colloid exclusion from the lower-velocity regions results in reduced dispersion of colloid particles, but if the reduction of the colloid effective porosity is substantial, then an overall increase in colloid dispersion is expected.

All longitudinal dispersivity values determined in this study were plotted as a function of interstitial velocity in Figure 6, and subsequently were statistically analyzed. The H_0 hypothesis that the population regression is linear was accepted, and the F test's hypothesis that the slope is zero was rejected. The standard regression lines show that there is a gentle increase in longitudinal dispersivity with increasing interstitial velocity. This observation is in agreement with the theoretical results published by *Liu and Kitanidis* [2013]. Figure 6 also suggests that colloid dispersivity is influenced by the column length. Note that dispersivity values determined from experiments conducted in 30 cm columns are in general slightly higher than those obtained from 15 cm columns. This result is consistent with the conventional assumption that dispersivity increases with scale [*Neuman*, 1990; *Gelhar et al.*, 1992].

The masses of colloids retained in the packed column for each of the transport experiments conducted in this study were estimated with (16), listed in Table 1, and plotted in Figure 7. Although in this study, the experimental procedures were specifically designed so that the colloid particles were not retained within the packed columns by attachment onto the glass beads, straining, and wedging, it is evident from Figure 7

Figure 7. Mass recovery as a function of colloid particle diameter. The squares represent colloid transport experiments conducted in 15 cm columns, and the circles colloid transport experiments conducted in 30 cm columns.
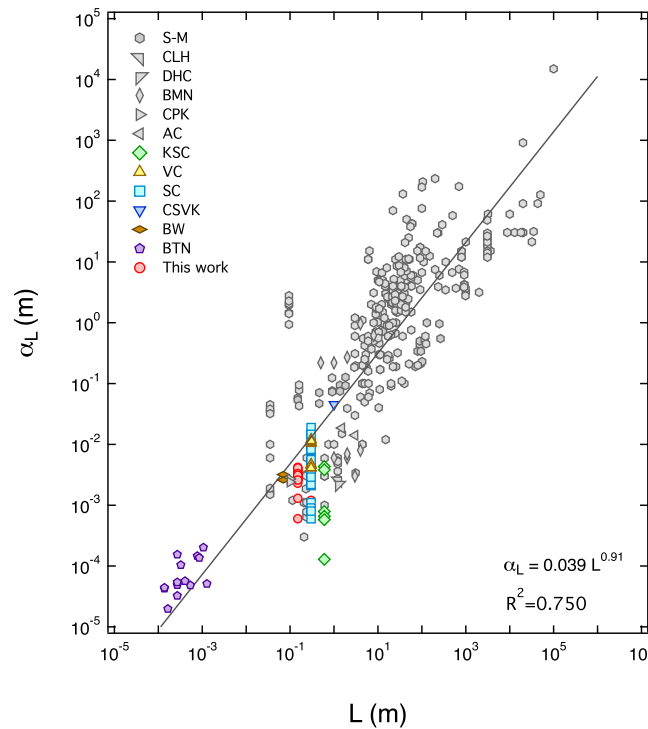
Figure 8. Compilation of 432 longitudinal dispersivities as a function of length scale. Molecular sized solutes are represented by gray symbols, and colloids/bio-colloids by various colored symbols. The solid line is a standard linear regression line. (S-M [*Schulze-Makuch*, 2005], CLH [*Chrysikopoulos et al.*, 2000], DHC [*Dela Barre et al.*, 2002], BMN [*Baumann et al.*, 2002], CPK [*Chrysikopoulos et al.*, 2011], AC [*Anders and Chrysikopoulos*, 2005], KSC [*Keller et al.*, 2004], VC [*Vasiliadou and Chrysikopoulos*, 2011], SC [*Syngouna and Chrysikopoulos*, 2011], CSVK [*Chrysiko-poulos et al.*, 2012], BW [*Baumann and Werth*, 2004], and BTN [*Baumann et al.*, 2010]).
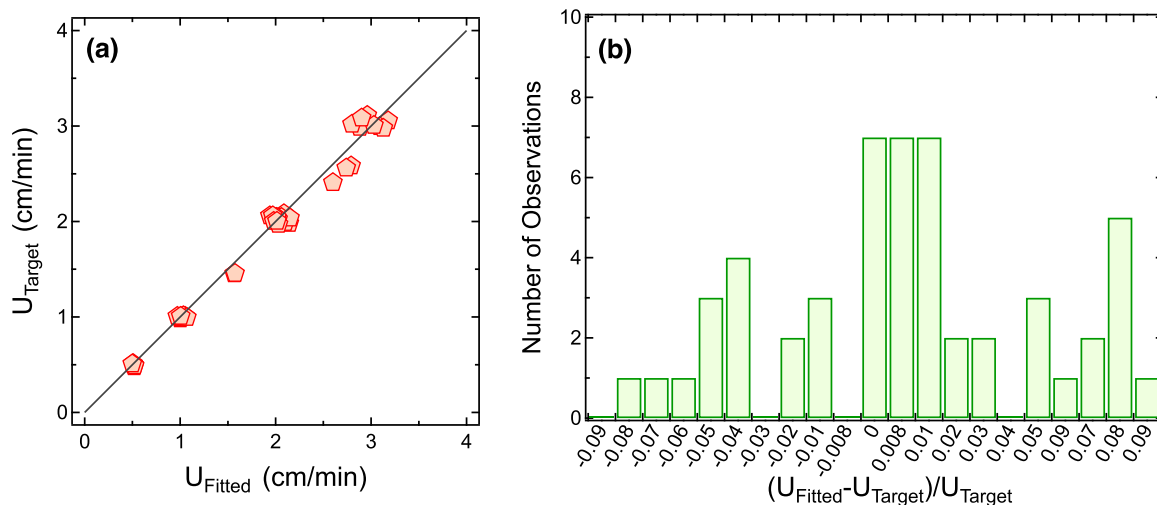
that a relatively small fraction of the larger size colloids were retained in the packed columns. Consequently, the dispersivities presented for the larger colloids employed in this study could be slightly underestimated.

Furthermore, an extensive compilation of a total of 380 dispersivity values from solute, colloid, and biocolloid studies at various scales were combined together with 52 dispersivity values from this study in Figure 8. The data assembled in Figure 8 suggest that that there is a strong overall trend of increasing dispersivity with displacement distance (scale). Certainly, this result is not novel but it is based on more data values than any previous study. The temptation was great to identify a single universal line by applying linear regression to all the data of Figure 8. The fitted line was of the form:

$$\alpha_L[m] = 0.039(L[m])^{0.91} \qquad (18)$$

It should be noted that in Figure 8, the displacement distance spans several orders of magnitude and covers data from the pore scale to field scale. The fitted parameter $\xi = 0.039$ ($m^{0.09}$) and the slope of the fitted line on log-log plot $\psi = 0.91$ compare well with the parameters ($\xi = 0.063$ ($m^{0.06}$) and $\psi = 0.94$)

reported by *Schulze-Makuch*, [2005]. Other values for the parameters ξ and ψ reported in the literature include: $\xi = 0.0175$ ($m^{-0.46}$), $\psi = 1.46$ based on selected "reliable" dispersivity data [*Neuman*, 1990], and $\xi = 0.1$, $\psi = 1$ based on a large portion of the available data [*Baumann et al.*, 2010]. The parameter values

Figure 9. Comparison between the target interstitial velocities (based on Q) and fitted colloid particle velocities: (a) scatterlot of variables U_{Target} and U_{Fitted}, and (b) histogram of ($U_{Fitted} - U_{Target}$)/U_{Target}. The solid line represents the ideal one-to-one correlation ($R^2 = 1$).
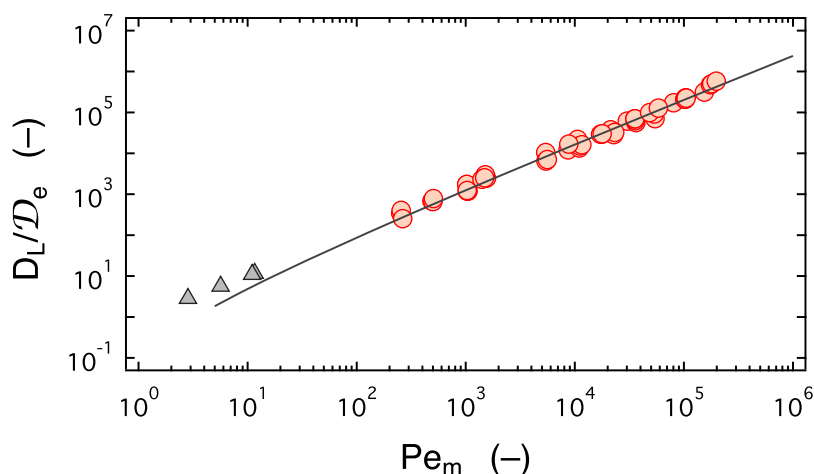
Figure 10. Scaling of the longitudinal hydrodynamic dispersion coefficients (circles for colloids, and triangles for tracer) with Péclet number. The solid line represents the correlation (19) reported by *Delgado* [2007].

for ξ and ψ obtained in this study can be considered as more reliable because they are based on 432 longitudinal dispersivity values, compared to the parameter values reported in previous studies, which were based on smaller data sets.

In order to detect the existence of either experimental artifacts or systematic errors in this study, the experimental data were subjected to comparisons. First, the interstitial velocities based on the flow rate set by the peristaltic pump, column porosity, and column cross-sectional area (U_{Target}), which are listed in Table 1, were directly compared with the fitted colloid particle velocities (U_{Fitted}) in Figure 9. The histogram of (U_{Fitted}-U_{Target})/U_{Target} (see Figure 9b) suggests that, for the majority of the experiments conducted in this study, U_{Fitted} is equal to or greater than U_{Target} ($U_{Fitted} \geq U_{Target}$). This is an expected result because colloids due to their finite size often flow faster than the average interstitial velocity. The fewer cases were $U_{Fitted} < U_{Target}$ (see Figure 9b) are attributed to possible tortuosity increase caused by the effective porosity reduction and to experimental errors, which are practically unavoidable in experimental work and particularly in experiments conducted in porous media. The observed colloid particle velocity increase is not very significant, mainly due to the uniform packing and relatively short length of the columns used in this study. Certainly, more significant colloid velocity enhancement would be observed in heterogeneous porous media and in longer packed columns. Next, the dimensionless Péclet number $Pe_m = Ud_c/\mathcal{D}_e$ for all transport experiments conducted in this study was determined and listed in Table 1. The Pe_m values range between 250 and 10^5, suggesting that the effect of molecular diffusion is negligible and mechanical dispersion is the governing dispersion process. As shown in Figure 10, the experimentally determined $D_L/\mathcal{D}_e$ values scale linearly with Pe_m. It is worthy to note that the following correlation suggested by *Delgado* [2007]:

$$\frac{D_L}{\mathcal{D}_e} = \frac{Pe_m}{6}\left[ln\left(\frac{3\tau}{2}Pe_m\right) - \frac{1}{4}\right], \qquad Pe_m \gg 1 \qquad (19)$$

fits surprisingly well the colloid dispersion data. The tracer data are outside the range ($Pe_m \gg 1$) of correlation validity. The comparisons presented in Figures 9 and 10 suggest that neither experimental artifacts nor systematic errors exist in the present study. Furthermore, a sensitivity analysis of the fitted model parameters was conducted to evaluate how changes in the best fitted parameter values can affect the objective function S, defined in (13). The two fitted parameters were fluctuated by $\pm 20\%$ and the corresponding impact on S was determined. It was found that the calculated S absolute values for U were in the range 26.2–971.4, and for D_L in the range 0.4–10.1. Obviously, U is the most sensitive of the two fitted parameters.

6. Conclusions

This study provided convincing experimental evidence that colloid dispersivity is not only a function of scale, as conventionally assumed, but also a function of colloid diameter and interstitial velocity. It was

shown that dispersivity increases linearly with increasing colloid particle size. This phenomenon was attributed to colloid dispersion enhancement due to possible reduction of the colloid effective porosity, which overbalances the reduction of colloid dispersion caused by colloid exclusion from the lower-velocity regions. A very important implication of this finding is that fitted dispersion coefficients based on tracer data should not be used to analyze colloid experimental data. Furthermore, the universal line (18) should be used with caution and not be routinely employed for longitudinal dispersivity value estimation.

References

Acharya, R. C., A. J. Valocchi, C. J. Werth, and T. W. Willingham (2007), Pore-scale simulation and reaction along a transverse mixing zone in two-dimensional porous media, *Water Resour. Res.*, *43*, W10435, doi:10.1029/2007WR005969.

Ahfir, N.-D., A. Benamar, A. Alem, and H. Wang (2009), Influence of internal structure and medium length on transport and deposition of suspended particles: A laboratory study, *Transp. Porous Media*, *76*, 289–307.

Anders, R., and C. V. Chrysikopoulos (2005), Virus fate and transport during artificial recharge with recycled water, *Water Resour. Res.*, *41*, W10415, doi:10.1029/2004WR003419.

Auset, M., and A. A. Keller (2004), Pore-scale processes that control dispersion of colloids in saturated porous media, *Water Resour. Res.*, *40*, W03503, doi:10.1029/2003WR002800.

Bales, R. C., C. P. Gerba, G. H. Grondin, and S. L. Jensen (1989), Bacteriophage transport in sandy soil and fractured tuff, *Appl. Environ. Microbiol.*, *55*, 2061–2067.

Baumann, T., and C. J. Werth (2004), Visualization and modeling of polystyrol colloid transport in silicon micromodel, *Vadose Zone J.*, *3*, 434–443.

Baumann, T., S. Müller, and R. Niessner (2002), Migration of dissolved heavy metal compounds and PCP in the presence of colloids through a heterogeneous calcareous gravel and a homogeneous quartz sand—Pilot scale experiments, *Water Res.*, *36*, 1213–1223.

Baumann, T., L. Toops, and R. Niessner (2010), Colloid dispersion on the pore scale, *Water Res.*, *44*, 1246–1254.

Bear, J. (1979), *Hydraulics of Groundwater*, McGraw-Hill, N. Y.

Bennacer, L., N.-D. Ahfir, A. Bouanani, A. Alem, and H. Wang (2013), Suspended particles transport and deposition in saturated granular porous medium: Particle size effects, *Transp. Porous Media*, *100*, 377–392.

Bird, R. B., W. E. Stewart, and E. N. Lightfoot (2002), *Transport Phenomena*, 2nd ed., John Wiley, N. Y.

Bradford, S. A., and M. Bettahar (2006), Concentration dependent transport of colloids in saturated porous media, *J. Contam. Hydrol.*, *82*, 99–117.

Bruggeman, D. A. G. (1935), Berechnung verschiedener physikalischer Konstanten von heterogenen Substanzen, *Ann. Phys.*, *24*, 636–679.

Brusseau, M. L. (1993), The influence of solute size, pore water velocity, and intraparticle porosity on solute dispersion and transport in soil, *Water Resour. Res.*, *29*(4), 1071–1080.

Chiogna, G., C. Eberhardt, P. Grathwohl, O. A. Cirpka, and M. Rolle (2010), Evidence of compound-dependent hydrodynamic and mechanical transverse dispersion by multitracer laboratory experiments, *Environ. Sci. Technol.*, *44*, 688–693.

Chrysikopoulos, C. V. (1993), Artificial tracers for geothermal reservoir studies, *Environ. Geol.*, *22*, 60–70.

Chrysikopoulos, C. V., and A. Abdel-Salam (1997), Modeling colloid transport and deposition in saturated fractures, *Colloids Surf. A*, *121*, 189–202, doi:10.1016/S0927–7757(96)03979-9.

Chrysikopoulos, C. V., and T.-J. Kim (2000), Local mass transfer correlations for nonaqueous phase liquid pool dissolution in saturated porous media, *Transp. Porous Media*, *38*(1/2), 167–187, doi:10.1023/A:1006655908240.

Chrysikopoulos, C. V., and V. I. Syngouna (2014), Effect of gravity on colloid transport through water-saturated columns packed with glass beads: Modeling and experiments, *Environ. Sci. Technol.*, *48*, 6805–6813, doi:10.1021/es501295n.

Chrysikopoulos, C. V., P. V. Roberts, and P. K. Kitanidis (1990), One-dimensional solute transport in porous media with partial well-to-well recirculation: Application to field experiments, *Water Resour. Res.*, *26*(6), 1189–1195, doi:10.1029/89WR03629.

Chrysikopoulos, C. V., P. K. Kitanidis, and P. V. Roberts (1992a), Generalized Taylor-Aris moment analysis of the transport of sorbing solutes through porous media with spatially-periodic retardation factor, *Transp. Porous Media*, *7*(2), 163–185, doi:10.1007/BF00647395.

Chrysikopoulos, C. V., P. K. Kitanidis, and P. V. Roberts (1992b), Macrodispersion of sorbing solutes in heterogeneous porous formations with spatially periodic retardation factor and velocity field, *Water Resour. Res.*, *28*(6), 1517–1529, doi:10.1029/92WR0001.

Chrysikopoulos, C. V., E. A. Voudrias, and M. M. Fyrillas (1994), Modeling contaminant transport resulting from dissolution of nonaqueous phase liquid pools in saturated porous media, *Transp. Porous Media*, *16*, 125–145, doi:10.1007/BF00617548.

Chrysikopoulos, C. V., K. Y. Lee, and T. C. Harmon (2000), Dissolution of a well-defined trichloroethylene pool in saturated porous media: Experimental design and aquifer characterization, *Water Resour. Res.*, *36*(7), 1687–1696, doi:10.1029/2000WR900082.

Chrysikopoulos, C. V., P.-Y. Hsuan, M. M. Fyrillas, and K. Y. Lee (2003), Mass transfer coefficient and concentration boundary layer thickness for a dissolving NAPL pool in porous media, *J. Hazard. Mater.*, *B97*, 245–255, doi:10.1016/S0304–3894(02)00264-9.

Chrysikopoulos, C. V., C. C. Plega, and V. E. Katzourakis (2011), Non-invasive in situ concentration determination of fluorescent or color tracers and pollutants in a glass pore network model, *J. Hazard. Mater.*, *198*, 299–306, doi:10.1016/j.hazmat.2011.10.042.

Chrysikopoulos, C. V., V. I. Syngouna, I. A. Vasiliadou, and V. E. Katzourakis (2012), Transport of *Pseudomonas putida* in a three-dimensional bench scale experimental aquifer, *Transp. Porous Media*, *94*, 617–642, doi:10.1007/s11242-012-0015-z.

Cirpka, O. A., A. Olsson, Q. Ju, M. A. Rahman, and P. Grathwohl (2006), Determination of transverse dispersion coefficients from reactive plume lengths, *Ground Water*, *44*(2), 212–221.

Dela Barre, B. K., T. C. Harmon, and C. V. Chrysikopoulos (2002), Measuring and modeling the dissolution of nonideally shaped dense nonaqueous phase liquid (NAPL) pools in saturated porous media, *Water Resour. Res.*, *38*(8), 1133, doi:10.1029/2001WR000444.

Delgado, J. M. P. Q. (2006), A critical review of dispersion in packed beds, *Heat Mass Transfer*, *42*, 279–310.

Delgado, J. M. P. Q. (2007), Longitudinal and transverse dispersion in porous media, *Chem. Eng. Res. Des.*, *85*(A9), 1245–1252.

Delgado, J. M. P. Q., and J. R. F. Guedes de Carvalho (2000), Measurement of the coefficient of transverse dispersion in flow through packed beds for a wide range of values of the Schmidt number, *Transp. Porous Media*, *44*, 165–180.

Doherty, J., L. Brebber, and P. Whyte (1994), *PEST: Model-Independent Parameter Estimation*, Watermark Comput., Brisbane, Australia.

Dong, H., T. C. Onstott, M. F. Deflaun, M. E. Fuller, T. D. Scheibe, S. H. Streger, R. K. Rothmel, and B. J. Mailloux (2002), Relative dominance of physical versus chemical effects on the transport of adhesion-deficient bacteria in intact cores from South Oyster, Virginia, *Environ. Sci. Technol.*, *36*, 891–900.

Fontes, D. E., A. L. Mills, G. M. Hornberger, and J. Herman (1991), Physical and chemical factors influencing transport of microorganisms through porous media, *Appl. Eviron. Microbiol.*, *57*(9), 2473–2481.

Gannon, J. T., V. B. Manilal, and M. Alexander (1991), Relationship between cell surface properties and transport of bacteria through soil, *Appl. Eviron. Microbiol.*, *57*(1), 190–193.

Garrouch, A. A., L. Ali, and F. Qasem (2001), Using diffusion and electrical measurements to assess tortuosity of porous media, *Ind. Eng. Chem. Res.*, *40*, 4363–4369.

Gelhar, L. W., and C. L. Axness (1983), Three-dimensional stochastic analysis of macrodispersion in aquifers, *Water Resour. Res.*, *19*(1), 161–180.

Gelhar, L. W., C. Welty, and K. R. Rehfeldt (1992), A critical review of data on field-scale dispersion in aquifers, *Water Resour. Res.*, *28*(7), 1955–1974.

Ginn, T. R. (2002), A travel time approach to exclusion on transport in porous media, *Water Resour. Res.*, *38*(4), 1041, doi:10.1029/2001WR000865.

Grindrod, P., M. S. Edwards, J. J. W. Higgo, and G. M. Williams (1996), Analysis of colloid and tracer breakthrough curves, *J. Contam. Hydrol.*, *21*, 243–253.

Han, N.-W., J. Bhakta, and R. G. Carbonell (1985), Longitudinal and lateral dispersion in packed beds: Effect of column length and particle size distribution, *AIChE J.*, *31*(2), 277–288.

Harleman, D. R. F., and R. R. Rumer (1963), Longitudinal and lateral dispersion in an isotropic porous medium, *J. Fluid Mech.*, *16*, 385–394.

Hu, Q., and M. L. Brusseau (1994), The effect of solute size on diffusive-dispersive transport in porous media, *J. Hydrol.*, *158*, 305–317.

Hu, Q., and M. L. Brusseau (1995), Effect of solute size on transport in structured porous media, *Water Rresour. Res.*, *31*(7), 1637–1646.

Icardi, M., G. Boccardo, D. L. Marchisio, T. Tosco, and R. Sethi (2014), Pore-scale simulation of fluid flow and solute dispersion in three-dimsnsional porous media, *Phys. Rev. E*, *90*, 013032.

James, S. C., and C. V. Chrysikopoulos (2000), Transport of polydisperse colloids in a saturated fracture with spatially variable aperture, *Water Resour. Res.*, *36*(6), 1457–1465, doi:10.1029/2000WR900048.

James, S. C., and C. V. Chrysikopoulos (2003), Effective velocity and effective dispersion coefficient for finite-sized particles flowing in a uniform fracture, *J. Colloid Interface Sci.*, *263*, 288–295, doi:10.1016/S0021-9797(03)00254-6.

James, S. C., and C. V. Chrysikopoulos (2011), Monodisperse and polydisperse colloid transport in water-saturated fractures with various orientations: Gravity effects, *Adv. Water Resour.*, *34*, 1249–1255, doi:10.1016/j.advwatres.2011.06.001.

Johnson, W. P., E. Pazmino, and H. Ma (2010), Direct observations of colloid retention in granular media in the presence of energy barriers, and implications for inferred mechanisms from indirect observations, *Water Res.*, *44*, 1158–1169.

Jourak, A., V. Frishfelds, J. G. I. Hellström, T. S. Lundström, I. Herrmann, and A. Hendström (2013), Longitudinal dispersion coefficient: Effects of particle-size distribution, *Transp. Porous Media*, *99*, 1–16.

Katzourakis, V. E., and C. V. Chrysikopoulos (2014), Mathematical modeling of colloid and virus cotransport in porous media: Application to experimental data, *Adv. Water Resour.*, *68*, 62–73, doi:10.1016/j.advwatres.2014.03.001.

Keller, A. A., S. S. Sirivithayapakorn, and C. V. Chrysikopoulos (2004), Early breakthrough of colloids and bacteriophage MS2 in a water-saturated sand column, *Water Resour. Res.*, *40*, W08304, doi:1029/2003WR002676.

Koch, D. C., and J. F. Brady (1985), Dispersion in fixed beds, *J. Fluid Mech.*, *134*, 399–427.

Liu, Y., and P. K. Kitanidis (2013), A mathematical and computational study of the dispersivity tensor in anisotropic porous media, *Adv. Water Resour.*, *62*, 303–316.

Maier, R. S., D. M. Kroll, R. S. Bernard, S. E. Howington, J. F. Peters, and H. T. Davis (2000), Pore-scale simulation of dispersion, *Phys. Fluids*, *12*(8), 2065–2079.

Morley, L. M., G. M. Hornberger, A. L. Mills, and J. S. Herman (1998), Effects of transverse mixing on transport of Bacteria through heterogeneous porous media, *Water Resour. Res.*, *34*(8), 1901–1908.

Neuman, S. P. (1990), Universal scaling of hydraulic conductivities in geologic media, *Water Resour. Res.*, *26*(8), 1749–1758.

Neuman, S. P. (1991), Reply to comments on ''Universal scaling of hydraulic conductivities and dispersivities in geologic media'' by M. P. Anderson, *Water Resour. Res.*, *27*(6), 1384–1385.

Olsson, A., and P. Grathwohl (2007), Transverse dispersion of non-reactive tracers in porous media: A new nonlinear relationship to predict dispersion coefficients, *J. Contam. Hydrol.*, *92*, 149–161.

Pickens, J. F., and G. E. Grisak (1981), Scale-dependent dispersion in a stratified granular aquifer, *Water Resour. Res.*, *17*(4), 1191–1211.

Pisani, L. (2011), Simple expression for the tortuosity of porous media, *Transp. Porous Media*, *88*, 193–203.

Powelson, D. K., C. P. Gerba, and M. T. Yahya (1993), Virus transport and removal in wastewater during aquifer recharge, *Water Res.*, *27*(4), 583–590.

Rahman, M. A., S. C. Jose, W. Nowak, and O. A. Cirpka (2005), Experiments on vertical transverse mixing in a large-scale heterogeneous model aquifer, *J. Contam. Hydrol.*, *80*. 130–148.

Rolle, M., G. Chiogna, R. Bauer, C. Griebler, and P. Grathwohl (2010), Isotopic fractionation by transverse dispersion: Flow-through microcosmos and reactive transport modeling study, *Environ. Sci. Technol.*, *44*, 6167–6173.

Russel, W. B., D. A. Saville, and W. R. Schowlter (1989), *Colloidal Dispersions*, 525 pp., Cambridge Univ. Press, Cambridge, U. K.

Salles, J., J. F. Thovert, and P. M. Adler (1993), Reconstructed porous media and their application to fluid flow and solute transport, *J. Contam. Hydrol.*, *13*(1–4), 3–22.

Scheibe, T. D., and B. D. Wood (2003), A particle-based model of size or anion exclusion with application to microbial transport in porous media, *Water Resour. Res.*, *39*(4), 1080, doi:10.1029/2001WR001223.

Schulze-Makuch, D. (2005), Longitudinal dispersivity data and implications for scaling behavior, *Ground Water*, *43*(3), 443–456.

Semprini, L., and P. L. McCarty (1991), Comparison between model simulations and field results for in-situ biorestoration of chlorinated aliphatics: Part 1, Biostimulation of methanotrophic bacteria, *Ground Water*, *29*(3), 365–374.

Sim, Y., and C. V. Chrysikopoulos (1995), Analytical models for one-dimensional virus transport in saturated porous media, *Water Resour. Res.*, *31*(5), 1429–1437, doi:10.1029/95WR00199.

Sim, Y., and C. V. Chrysikopoulos (1998), Three-dimensional analytical models for virus transport in saturated porous media, *Transp. Porous Media*, *30*(1), 87–112, doi:10.1023/A:1006596412177.

Sim, Y., and C. V. Chrysikopoulos (1999), Analytical solutions for solute transport in saturated porous media with semi-infinite or finite thickness, *Adv. Water Resour.*, *22*(5), 507–519, doi:10.1016/S0309-1708(98)00027-X.

Sinton, L. W., M. L. Mackenzie, N. Karki, R. L. Dann, L. Pang, and M. E. Close (2012), Transport of Escherichia coli and F-RNA bacteriophages in a 5-m column of saturated, heterogeneous gravel, *Water Air Soil Pollut.*, *223*, 2347–2360.

Syngouna, V. I., and C. V. Chrysikopoulos (2011), Transport of biocolloids in water saturated columns packed with sand: Effect of grain size and pore water velocity, *J. Contam. Hydrol.*, *126*, 301–314, doi:10.1016/j.jconhyd.2011.09.007.

Syngouna, V. I., and C. V. Chrysikopoulos (2013), Cotransport of clay colloids and viruses in water saturated porous media, *Colloids Surf. A*, *416*, 56–65, doi:10.1016/j.colsurfa.2012.10.018.

Thomas, J. M., and C. V. Chrysikopoulos (2007), Experimental investigation of acoustically enhanced colloid transport in water-saturated packed columns, *J. Colloid Interface Sci.*, *308*, 200–207, doi:10.1016/j.jcis.2006.12.062.

Tong, M., X. Li, C. N. Brow, and W. P. Johnson (2005), Detachment influenced transport of an adhesion-deficient bacterial strain within water-reactive porous media, *Environ. Sci. Technol.*, *39*, 2500–2508.

Toran, L., and A. V. Palumbo (1992), Colloid transport through fractured and unfractured laboratory sand columns, *J. Contam. Hydrol.*, *9*, 289–303.

van Milligen, B. Ph., and P. D. Bons (2012), Analytical model for tracer dispersion in porous media, *Phys. Rev. E*, *85*, 011306.

Vasiliadou, I. A., and C. V. Chrysikopoulos (2011), Cotransport of *Pseudomonas putida* and kaolinite particles through water saturated columns packed with glass beads, *Water Resour. Res.*, *47*, W02543, doi:10.1029/2010WR009560.

Whitaker, S. (1986), Flow in porous media II: The governing equations of immiscible, two-phase flow, *Transp. Porous Media 1*, 105–125.

Wilke, C. R., and P. Chang (1955), Correlation of diffusion coefficients in dilute solutions, *AIChE J.*, *1*, 264–270.